

# Hidden-symmetry-protected $Z_2$ topological insulator in a cubic lattice

Jing-Min Hou<sup>1,\*</sup> and Wei Chen<sup>2</sup>

<sup>1</sup>*School of Physics, Southeast University, Nanjing 211189, China*

<sup>2</sup>*College of Science, Nanjing University of Aeronautics and Astronautics, Nanjing 210016, China*

Usually  $Z_2$  topological insulators are protected by time reversal symmetry. Here, we present a new type of  $Z_2$  topological insulators in a cubic lattice which is protected by a novel hidden symmetry, while time reversal symmetry is broken. The hidden symmetry has a composite antiunitary operator consisting of fractional translation, complex conjugation, sublattice exchange, and local gauge transformation. Based on the hidden symmetry, we define the hidden-symmetry polarization and  $Z_2$  topological invariant to characterize the topological insulators. The surface states have band structures with odd number of Dirac cones, where pseudospin-momentum locking occurs. When the hidden-symmetry-breaking perturbations are added on the boundaries, a gap opens in the surface band structure, which confirms that the topological insulator and the surface states are protected by the hidden symmetry. We also discuss the realization and detection of this new kind of  $Z_2$  topological insulator in optical lattices with ultracold atom techniques.

## I. INTRODUCTION

Recently, topological phases in condensed matters attract much attention of physicists[1, 2]. Before 1980s, it was believed that matter is classified by symmetries according to Landau's theory. The discovery of the quantum Hall effect overturned that belief since two distinct quantum Hall insulators may have the same symmetry[3]. Very soon, it was realized that quantum Hall insulators are classified by a topological invariant, i.e., the Chern number, which is directly related to the quantized Hall conductivity[4]. Thus, quantum Hall insulators are time-reversal-symmetry-breaking topological phases due to the existence of magnetic field. Since then, the door of the study of topological phases in condensed matter physics was opened. Later, the discoveries of  $Z_2$  topological insulators in two and three dimensions significantly boom the research on topological phases in condensed matter physics[5–19]. In general, the  $Z_2$  topological insulators are induced by spin-orbit coupling and protected by time reversal symmetry. Such nontrivial phases are characterized by the topological edge or surface states, which exhibit spin-momentum locking.

Besides time-reversal-symmetry-protected topological insulators, there are also topological insulators protected by spatial symmetry (i.e. topological crystalline insulators) that have been predicted theoretically and prepared experimentally[20–22]. Recently, we found a kind of hidden symmetry which protects the degeneracies at Dirac points of a square lattice[23, 24]. This kind of hidden symmetry is a composite antiunitary symmetry, generally consisting of fractional translation, complex conjugation, sublattice exchange, and local gauge transformation. We have found a two-dimensional optical lattice preserving this kind of hidden symmetry, which supports quantum pseudospin Hall effect, i.e., a  $Z_2$  two-dimensional topological insulator[25]. A natural question is whether the hidden symmetry supports the existence of  $Z_2$  topological insulators in three dimensions. In this paper, we will give a positive answer.

In the following sections, we propose a tight-binding model in a cubic lattice, which preserves a hidden symmetry, i.e., a composite antiunitary symmetry. Based on the hidden symmetry, the pseudospin, symmetry-polarization and  $Z_2$  topological invariant are defined. We calculate the dispersion relation of the system and find that the band inversions happen when changing the parameters across some fixed values. Based on the  $Z_2$  topological invariants and band inversions, the phase diagram is drawn. We evaluate the surface states of a slab geometry and calculate the pseudospin textures of the surface states. The insulator with non-trivial topological invariant has odd number of Dirac cones in the surface band structure, which have pseudospin-momentum-locking pseudospin textures. When the hidden-symmetry-breaking perturbations are added on the boundaries of the slab, a gap opens at the surface Dirac points and the surface states on the two opposite boundaries mix, even turn into bulk states when the perturbations are strong enough, which confirm that the topological insulator is protected by the hidden symmetry. The recent development of experimental techniques of ultracold atoms in optical lattices have make them become a platform to simulate the exotic physics in condensed matters[26–28]. Thus, we suggest to realize this model with ultracold atoms in optical lattices and to detect the topological properties with state-of-the-art techniques in cold atomic physics.

## II. MODEL

Here, we consider two-level atoms trapped in a cubic optical lattice as shown in Fig.1(a), where the arrows represent the hopping-accompanying phases. Due to the appearing of the hopping-accompanying phases, the translation symmetry is broken. Thus, the lattice is divided into two sublattices, i.e. sublattices  $A$  and  $B$ , denoted by the red and blue spheres in Fig.1(a), respectively. Taking the distance between the nearest lattice sites as the unit of length, we define the primitive lattice vectors as  $\mathbf{a}_1 = (1, -1, 0)$ ,  $\mathbf{a}_2 = (1, 1, 0)$ , and  $\mathbf{a}_3 = (0, 0, 1)$ . The primitive reciprocal lattice vectors are  $\mathbf{b}_1 = (\pi, -\pi, 0)$ ,  $\mathbf{b}_2 = (\pi, \pi, 0)$ , and  $\mathbf{b}_3 = (0, 0, 2\pi)$  and the corresponding Brillouin zone is shown in Fig.1(b). The system can be de-

\* Corresponding author: jmh@seu.edu.cn

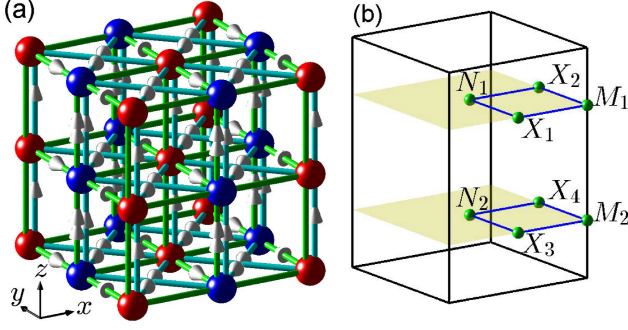


FIG. 1. (a) Schematic of the cubic lattice, where the red and blue spheres represent the lattice sites of sublattices  $A$  and  $B$ , respectively, and the green and cyan sticks represent the hoppings with the color transition matrices  $\tau_x$  and  $\tau_z$ , respectively, and the grey single arrows and double arrows denote the hopping-accompanying phases  $\pi/2$  and  $\pi$ , respectively. (b) The Brillouin zone, where the green spheres represent the hidden-symmetry-invariant points.

scribed by the tight-binding Hamiltonian  $H = H_0 + H_1 + H_2$  with

$$\begin{aligned}
 H_0 = & - \sum_{i \in A} [t_x \hat{a}_i^\dagger \tau_x \hat{b}_{i+\hat{x}} + t_x \hat{a}_i^\dagger \tau_x \hat{b}_{i-\hat{x}} \\
 & + t_y e^{-i\pi/2} \hat{a}_i^\dagger \tau_x \hat{b}_{i+\hat{y}} + t_y e^{-i\pi/2} \hat{a}_i^\dagger \tau_x \hat{b}_{i-\hat{y}} \\
 & + t_z \hat{a}_i^\dagger \tau_x \hat{a}_{i+\hat{z}} - t_z \hat{b}_{i+\hat{x}}^\dagger \tau_x \hat{b}_{i+\hat{x}+\hat{z}}] \\
 & + H.c.
 \end{aligned} \quad (1)$$

and

$$\begin{aligned}
 H_1 = & -t_1 \sum_{i \in A} [a_i^\dagger \tau_z a_{i+\hat{x}-\hat{y}} - a_i^\dagger \tau_z a_{i+\hat{x}+\hat{y}} + e^{-i\pi/2} a_i^\dagger \tau_z a_{i+\hat{z}}] \\
 & -t_1 \sum_{i \in B} [b_i^\dagger \tau_z b_{i+\hat{x}-\hat{y}} - b_i^\dagger \tau_z b_{i+\hat{x}+\hat{y}} + e^{-i\pi/2} b_i^\dagger \tau_z b_{i+\hat{z}}] \\
 & + H.c.
 \end{aligned} \quad (2)$$

and

$$H_2 = \lambda \sum_{i \in A} a_i^\dagger \tau_z a_i + \lambda \sum_{i \in B} b_i^\dagger \tau_z b_i \quad (3)$$

where  $a_i = [a_i^{(1)}, a_i^{(2)}]^T$  and  $b_i = [b_i^{(1)}, b_i^{(2)}]^T$  are the two-component annihilation operators destructing an atom at a lattice site of sublattice  $A$  and  $B$ , respectively;  $\tau_i$  ( $i = x, y, z$ ) represent the Pauli matrices in the color space spanned by the two atomic levels;  $t$  and  $t_1$  represent the amplitudes of hopping between the nearest lattice sites and between the next-nearest lattice sites, respectively;  $\lambda$  is the magnitude of an effective Zeeman term.

After the Fourier transformation, the Bloch Hamiltonian is obtained as

$$\begin{aligned}
 \mathcal{H}(\mathbf{k}) = & -2t \cos k_x \sigma_x \otimes \tau_x - 2t \cos k_y \sigma_y \otimes \tau_x \\
 & -2t \cos k_z \sigma_z \otimes \tau_x + m(\mathbf{k}) I \otimes \tau_z,
 \end{aligned} \quad (4)$$

where  $m(\mathbf{k}) = \lambda - 4t_1 \sin k_x \sin k_y - 2t_1 \sin k_z$  represents a mass term. Diagonalizing Eq.(4), we arrive at the dispersion

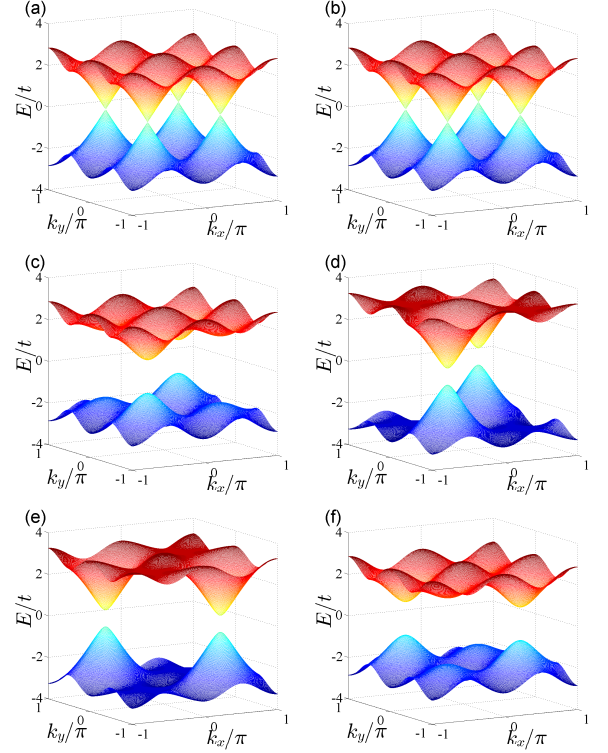


FIG. 2. The dispersion relations (a) on the  $k_z = \pi/2$  plane and (b) on the  $k_z = -\pi/2$  plane for  $t_1 = 0$  and  $\lambda = 0$ , (c) on the  $k_z = \pi/2$  plane and (d) on the  $k_z = -\pi/2$  plane for  $t_1 = 0.3t$  and  $\lambda = t$ , (e) on the  $k_z = \pi/2$  plane and (f) on the  $k_z = -\pi/2$  plane for  $t_1 = 0.3t$  and  $\lambda = -t$ .

relation as

$$E(\mathbf{k}) = \pm \sqrt{4t^2(\cos^2 k_x + \cos^2 k_y + \cos^2 k_z) + m(\mathbf{k})^2} \quad (5)$$

From the dispersion relation, it is found that the energy bands are two-fold degenerate for the conduction and valence bands. When Hamiltonians  $H_1$  and  $H_2$  disappear, the mass term vanishes and the conduction and valence bands touched at the points  $X_{1,2} = (\pi/2, \mp\pi/2, \pi/2)$  and  $X_{3,4} = (\pi/2, \mp\pi/2, -\pi/2)$  in the Brillouin zone as shown in Figs.2(a) and (b). When  $H_1$  and  $H_2$  appear, the mass term is non-zero, then a gap opens between the conduction and valence bands as shown in Figs.2(c)-(d). The masses at the Dirac points have different signs for different parameter ranges as shown in Table I. Based on the signs of masses at the Dirac points, they can be divided into eight parameter ranges: (i)  $\lambda > 6|t_1|$ , (ii)  $t_1 > 0$  and  $6t_1 > \lambda > 2t_1$ , (iii)  $|\lambda| < 2t_1$ , (iv)  $t_1 > 0$  and  $-2t_1 > \lambda > -6t_1$ , (v)  $\lambda < -6|t_1|$ , (vi)  $t_1 < 0$  and  $2t_1 > \lambda > 6t_1$ , (vii)  $|\lambda| < -2t_1$ , (viii)  $t_1 < 0$  and  $-6t_1 > \lambda > -2t_1$ . These insulators are classified by a  $Z_2$  topological invariant, which will be defined in Section IV. As one crosses the boundary between two neighboring parameter ranges, a band inversion happens at one of Dirac points, which indicates a topological phase transition. That is to say, the insulators in two neighboring parameter ranges belong to two distinct topological sectors. The insulators with odd number

	Parameter ranges	$X_1$	$X_2$	$X_3$	$X_4$
(i)	$\lambda > 6 t_1 $	+	+	+	+
(ii)	$t_1 > 0, 6t_1 > \lambda > 2t_1$	+	-	+	+
(iii)	$ \lambda  < 2t_1$	+	-	+	-
(vi)	$t_1 > 0, -2t_1 > \lambda > -6t_1$	-	-	+	-
(v)	$\lambda < -6 t_1 $	-	-	-	-
(vi)	$t_1 < 0, 2t_1 > \lambda > 6t_1$	-	+	-	-
(vii)	$ \lambda  < -2t_1$	-	+	-	+
(viii)	$t_1 < 0, -6t_1 > \lambda > -2t_1$	+	+	-	+

TABLE I. The sign of the masses at the Dirac points for different parameter ranges.

of negative masses at the Dirac points are topologically non-trivial insulators, while the ones with even number of negative masses at the Dirac points are trivial insulators, which will be confirmed in the succeeding sections of the paper. Therefore, the system is a  $Z_2$  topological insulator in parameter ranges (ii) (iv), (vi) and (viii) and is a trivial band insulator in parameter ranges (i), (iii), (v) and (vii) as shown in Fig.3.

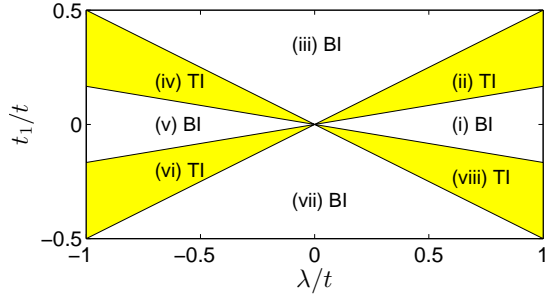


FIG. 3. The phase diagram of the cubic lattice. Here, TI and BI represent topological insulators and conventional band insulators, respectively.

### III. HIDDEN SYMMETRY

It is easy to verify that the system has a hidden symmetry with the symmetry operator as

$$\Upsilon = (e^{i\pi})^{i_z} (\sigma_x \otimes I) T_{\hat{x}} K \quad (6)$$

where  $K$  is the complex conjugate operator,  $T_{\hat{x}}$  is a translation operator that moves the lattice by a unit along the  $x$  direction,  $\sigma_x$  is the Pauli matrix representing sublattice exchange,  $I$  is the unit matrix in the color space, and  $(e^{i\pi})^{i_z}$  is a local  $U(1)$  gauge transformation and  $i_z$  is the  $z$ -component of the space coordinate. The Bloch functions are supposed to have the form  $\Psi_{\mathbf{k}}(\mathbf{r}) = [u_{A,\mathbf{k}}^{(1)}(\mathbf{r}), u_{A,\mathbf{k}}^{(2)}(\mathbf{r}), u_{B,\mathbf{k}}^{(1)}(\mathbf{r}), u_{B,\mathbf{k}}^{(2)}(\mathbf{r})]^T e^{i\mathbf{k}\cdot\mathbf{r}}$  in

the coordinate representation. The symmetry operator  $\Upsilon$  acts on the Bloch function as follows

$$\Upsilon \Psi_{\mathbf{k}}(\mathbf{r}) = \begin{pmatrix} u_{B,\mathbf{k}}^{(1)*}(\mathbf{r} - \hat{x}) e^{ik_x} \\ u_{B,\mathbf{k}}^{(2)*}(\mathbf{r} - \hat{x}) e^{ik_x} \\ u_{A,\mathbf{k}}^{(1)*}(\mathbf{r} - \hat{x}) e^{ik_x} \\ u_{A,\mathbf{k}}^{(2)*}(\mathbf{r} - \hat{x}) e^{ik_x} \end{pmatrix} e^{-i\mathbf{k}\cdot\mathbf{r} + i\pi i_z} = \Psi'_{\mathbf{k}'}(\mathbf{r}) \quad (7)$$

Because  $\Upsilon$  is the symmetry operator of the system,  $\Psi'_{\mathbf{k}'}(\mathbf{r})$  must be a Bloch function of the system. Thus, we obtain  $\mathbf{k}' = (-k_x, -k_y, -k_z + \pi)$ ,  $u_{A,\mathbf{k}'}^{(n)}(\mathbf{r}) = u_{B,\mathbf{k}}^{(n)*}(\mathbf{r} - \hat{x}) e^{ik_x}$  and  $u_{B,\mathbf{k}'}^{(n)}(\mathbf{r}) = u_{A,\mathbf{k}}^{(n)*}(\mathbf{r} - \hat{x}) e^{ik_x}$  with  $n = 1, 2$ . Thus, one can find that the symmetry operator  $\Upsilon$  acts on the wave vector as

$$\Upsilon : \mathbf{k} = (k_x, k_y, k_z) \rightarrow \mathbf{k}' = (-k_x, -k_y, -k_z + \pi)$$

If  $\mathbf{k}' = \mathbf{k} + \mathbf{G}$ , where  $\mathbf{G}$  is a reciprocal lattice vector, then we can say that  $\mathbf{k}$  is a  $\Upsilon$ -invariant point in momentum space. There are eight distinct  $\Upsilon$ -invariant points as  $X_{1,2,3,4} = (\pi/2, \pm\pi/2, \pm\pi/2)$ ,  $N_{1,2} = (0, 0, \pm\pi/2)$ , and  $M_{1,2} = (0, \pi, \pm\pi/2)$  in the Brillouin zone as shown in Fig.1(b). From Eq.(6), we obtain that the square of the hidden symmetry operator is  $\Upsilon^2 = T_{2\hat{x}}$ , which has the representation based on the Bloch functions as  $\Upsilon^2 = e^{-i2\mathbf{k}\cdot\hat{x}}$ . Therefore, we have  $\Upsilon^2 = -1$  at points  $X_{1,2,3,4}$  while  $\Upsilon^2 = 1$  at points  $N_{1,2}$  and  $M_{1,2}$  in the Brillouin zone. Furthermore, since  $\Upsilon$  is an antiunitary operator, there must exist two-fold degeneracies at points  $X_{1,2,3,4}$ , which are protected by the hidden symmetry  $\Upsilon$ [23].

### IV. $Z_2$ TOPOLOGICAL INVARIANT

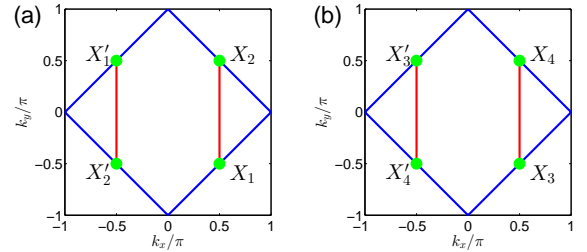


FIG. 4. The integration paths for the definition of charge polarization on (a) the  $k_z = \pi/2$  and (b)  $k_z = -\pi/2$  planes in the Brillouin zone. Here, the red lines represent the integration paths and  $X_i$  and  $X'_i$  represent the  $\Upsilon$ -invariant points at which hidden-symmetry-protected degeneracies appear.

Based on the hidden symmetry  $\Upsilon$ , we can define a  $Z_2$  topological invariant, which is used to classify the insulator phases of the system. The Bloch functions of the occupied bands can be written as  $|\Psi_{n,\mathbf{k}}\rangle = e^{i\mathbf{k}\cdot\mathbf{r}} |u_{n,\mathbf{k}}\rangle$ , where  $|u_{n,\mathbf{k}}\rangle$  is the the cell-periodic eigenstate of the Bloch Hamiltonian  $\mathcal{H}(\mathbf{k})$ . The Berry connection matrix is defined as

$$\mathbf{a}_{mn} = -i \langle u_{m,\mathbf{k}} | \nabla_{\mathbf{k}} | u_{n,\mathbf{k}} \rangle \quad (8)$$

For the hidden symmetry  $\Upsilon$ , we also define a matrix as

$$w_{mn}(\mathbf{k}) = \langle u_{m,\mathbf{k}'} | \Upsilon | u_{n,\mathbf{k}} \rangle \quad (9)$$

where  $\mathbf{k}'$  is the wave vector by  $\Upsilon$  acting on  $\mathbf{k}$ , i.e.,  $\mathbf{k}' = (-k_x, -k_y, -k_z + \pi)$ . Since  $\Upsilon^2 = -1$  is satisfied at  $\Upsilon$ -invariant points  $X_{1,2,3,4}$  and  $\Upsilon$  is an antiunitary operator, it is easy to verify that  $w$  is an antisymmetric matrix at the  $\Upsilon$ -invariant degenerate points  $X_{1,2,3,4}$ .

For the present model with half filling, there are two occupied bands, which compose the  $\Upsilon$  pair bands. For the occupied  $\Upsilon$  pair bands, we define the charge polarization in terms of the Berry connection as

$$P_\rho^\pm = \frac{1}{2\pi} \left[ \int_{X_\alpha}^{X_\beta} \mathbf{A}(\mathbf{k}) \cdot d\mathbf{k} + \int_{X'_\alpha}^{X'_\beta} \mathbf{A}(\mathbf{k}) \cdot d\mathbf{k} \right] \quad (10)$$

where the integration is along the red lines on the  $k_z = \pi/2$  and  $k_z = -\pi/2$  planes of the Brillouin zone as shown in Fig.4;  $\mathbf{A}(\mathbf{k})$  is defined as  $\text{tr}[\mathbf{a}(\mathbf{k})]$ ; The signs  $\pm$  denote the  $k_z = \pi/2$  and  $k_z = -\pi/2$  planes, respectively;  $\alpha = 1, \beta = 2$  for the  $k_z = \pi/2$  plane and  $\alpha = 3, \beta = 4$  for the  $k_z = -\pi/2$  plane. For each occupied band, the partial charge polarization is defined as

$$P_i^\pm = \frac{1}{2\pi} \left[ \int_{X_\alpha}^{X_\beta} \mathbf{a}_{ii}(\mathbf{k}) \cdot d\mathbf{k} + \int_{X'_\alpha}^{X'_\beta} \mathbf{a}_{ii}(\mathbf{k}) \cdot d\mathbf{k} \right] \quad (11)$$

For the  $\Upsilon$  pair bands, we can also define the  $\Upsilon$  polarization as

$$\begin{aligned} P_\Upsilon^\pm &= P_1^\pm - P_2^\pm = 2P_1^\pm - P_\rho^\pm \\ &= \frac{1}{2\pi} \int_{X_\alpha}^{X_\beta} [\mathbf{A}(\mathbf{k}) - \mathbf{A}(\mathbf{k}')] \cdot d\mathbf{k} - \frac{i}{\pi} \log \frac{w_{12}(X_\beta)}{w_{12}(X_\alpha)} \\ &= \frac{1}{i\pi} \log \left[ \frac{\sqrt{w_{12}(X_\alpha)^2}}{w_{12}(X_\alpha)} \cdot \frac{w_{12}(X_\beta)}{\sqrt{w_{12}(X_\beta)^2}} \right] \end{aligned} \quad (12)$$

The Hilbert space can be classified into two groups depending on the difference between the  $\Upsilon$  polarizations on the  $k_z = \pi/2$  and  $k_z = -\pi/2$  planes,

$$\Delta = P_\Upsilon^+ - P_\Upsilon^- \quad (13)$$

The  $\Upsilon$  polarization is an integer and only defined modulo 2 due to the ambiguity of the log. The argument of the log has only two values  $\pm 1$  associated with the even and odd values of  $P_\Upsilon^\pm$ , respectively. Therefore, we can rewrite Eq.(13) as

$$(-1)^\Delta = \prod_{\alpha=1}^4 \frac{\text{Pf}[w(X_\alpha)]}{\sqrt{\det[w(X_\alpha)]}} \quad (14)$$

The  $Z_2$  topological invariant can be defined as  $\Delta$  modulo 2. When  $\Delta$  is odd or even, the system is a topological insulator or a trivial band insulator. Therefore, Eq.(14) gives a distinct definition of the  $Z_2$  topological invariant.

## V. SURFACE STATES AND THEIR PSEUDOSPIN TEXTURES

Generally, topological insulators have special surface states, for example, the surface bands have odd number of

Dirac cones in the corresponding surface Brillouin zone. Here, in order to manifest the surface states of the hidden-symmetry-protected  $Z_2$  topological insulator, we investigate a slab with open boundaries along the  $z$  direction. Based on the numerical results, it is found that there exists a single Dirac cone on the surface Brillouin zone for the topological insulator phases, which as shown in Fig.5 and Fig.6 for parameter ranges (ii) and (iv), respectively. In these two parameter ranges, the system is a topological insulator but the location of the surface Dirac point in the surface Brillouin zone are different. In parameter range (ii), the surface Dirac point locates at points  $(\pi/2, \pi/2)$  of the surface Brillouin zone as shown in Fig.5(a), while, in parameter range (iv), the surface Dirac point locates at point  $(-\pi/2, \pi/2)$  of the surface Brillouin zone as shown Fig.6(a). For every state on the surface Dirac cone, the distribution of probability density concentrate on one of the open boundaries as shown in Fig.5(b) and Fig.6(b). The Dirac cone surface states are two-fold degenerate, since they localize the opposite boundaries of the slab. When the quantum states are outside of the Dirac cone, they become bulk states, that is to say, the surface states only occur on the Dirac cone area of the surface Brillouin zone.

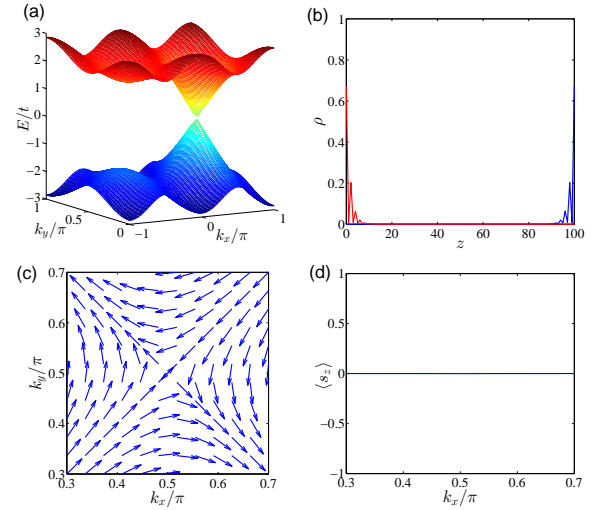


FIG. 5. The properties of the highest valence bands (surface states) of a slab preserving the hidden symmetry for the case  $t_1 = 0.3t$  and  $\lambda = t$ . (a) The dispersion relation; (b) the probability density of the surface states with the wave vector  $(k_x, k_y) = (0.6\pi, 0.5\pi)$ , where the red and blue lines correspond to the two degenerate states localized on the opposite open boundaries, respectively; (c) the pseudospin textures of the average pseudospin components  $(\langle s_x \rangle, \langle s_y \rangle)$  on the  $k_x$ - $k_y$  plane; (d) the profiles of the average component of pseudospin  $\langle s_z \rangle$  along the  $k_y = 0.5\pi$  line. Here, the two degenerate surface states localized on the two boundaries have the same pseudospin textures and the vanishing average pseudospin component  $\langle s_z \rangle$ .

In order to investigate the pseudospin texture of the surface states, we define the pseudospin operators as  $s_x = \frac{1}{2}\sigma_y \otimes \tau_x$ ,  $s_y = \frac{1}{2}\sigma_x \otimes \tau_x$ , and  $s_z = -\frac{1}{2}\sigma_z \otimes I$  with the commutation relations  $[s_i, s_j] = i\epsilon_{ijk}s_k$ . For the surface states, the pseudospins form a vortex or antivortex pseudospin texture

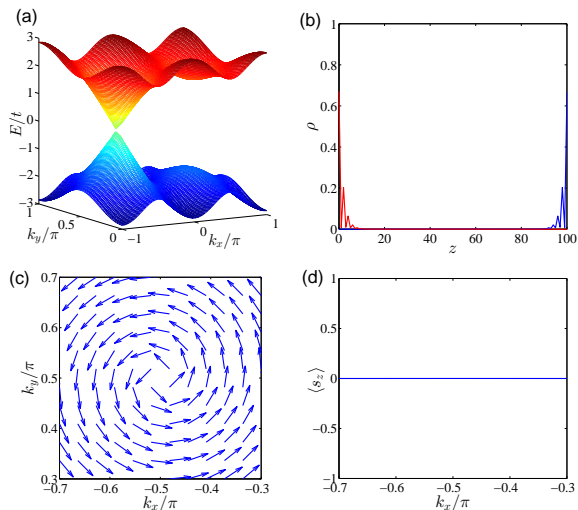


FIG. 6. The properties of the highest valence bands (surface states) of a slab preserving the hidden symmetry for the case  $t_1 = 0.3t$  and  $\lambda = -t$ . (a) The dispersion relation; (b) the probability density of the surface states with the wave vector  $(k_x, k_y) = (-0.6\pi, 0.5\pi)$ , where the red and blue lines correspond to the two degenerate states localized on the opposite open boundaries, respectively; (c) the pseudospin texture of the average pseudospin components ( $\langle s_x \rangle, \langle s_y \rangle$ ) on the  $k_x$ - $k_y$  plane; (d) the profile of the average component of pseudospin  $\langle s_z \rangle$  along the  $k_y = 0.5\pi$  line. Here, the two degenerate surface states localized on the two boundaries have the same pseudospin textures and the vanishing average pseudospin component  $\langle s_z \rangle$ .

on the surface Brillouin zone with a number number  $+1$  or  $-1$ , respectively. For the case in the parameter range (ii), Fig.5(c) shows the pseudospin texture of the average pseudospin components ( $\langle s_x \rangle, \langle s_y \rangle$ ) on the surface Brillouin zone and Fig.5(d) shows that the average pseudospin component  $\langle s_z \rangle$  is vanishing for the Dirac surface states. That is to say, there is a singularity at the surface Dirac points  $(-\pi/2, \pi/2)$  for the pseudospin texture. Integrating the Berry connection along a circle enclosed the Dirac point for a valence band surface state, one can obtain a  $\pi$  Berry phase, which can be used to define a winding number  $-1$ , so the pseudospin form an anti-vortex structure. For the case in parameter range (iv), Fig.6(c) and Fig.6(d) show the pseudospin texture of the average pseudospin components ( $\langle s_x \rangle, \langle s_y \rangle$ ) on the surface Brillouin zone and the average pseudospin component  $\langle s_z \rangle$ , respectively. Similarly, the only the in-plane pseudospin components ( $\langle s_x \rangle, \langle s_y \rangle$ ) exist and they form a vortex. The different point is that the vortex has a opposite winding number  $+1$ , compared with the case in the parameter range (ii). Beside the parameter ranges (ii) and (iv), the parameter ranges (vi) and (viii) also support the existence of  $Z_2$  topological insulators. The Dirac points have the same position and the surface states have the same pseudospin texture on the surface Brillouin zone for the parameter ranges (ii) and (vi), and for the parameter ranges (iv) and (viii), respectively.

## VI. THE EFFECTS OF THE HIDDEN-SYMMETRY-BREAKING PERTURBATIONS

Since the  $Z_2$  topological insulator and the surface states are protected by the hidden symmetry  $\Upsilon$ , the surface states should be gapped if some perturbations breaking the hidden symmetry  $\Upsilon$  are added on the boundaries of the lattice. In order to verify the protection by hidden symmetry  $\Upsilon$ , we add the hidden-symmetry-breaking perturbation terms on the two open boundaries of a slab and investigate the effects of these terms. We assume that the hidden-symmetry-breaking perturbations on the boundaries has the form,

$$H_p = \mu \sum_{i \in SA} a_i^\dagger a_i - \mu \sum_{j \in SB} b_j^\dagger b_j \quad (15)$$

where  $\mu$  is the magnitude of the perturbations;  $SA$  and  $SB$  denote the boundary surfaces of sublattice  $A$  and  $B$ . We calculate the dispersion relations, probability densities, and pseudospin textures for  $t_1 = 0.3t$ ,  $\lambda = t$ ,  $\mu = 0.8t$  and  $t_1 = 0.3t$ ,  $\lambda = -t$ ,  $\mu = 0.8t$ , which are shown in Fig.7 and Fig.8, respectively. Fig.7(a) and Fig.8(a) show the highest valence bands and the lowest conduction bands, which correspond to the surface states in the case without hidden-symmetry-breaking perturbations. It is found that the hidden-symmetry-breaking perturbations open a gap between the highest valence and lowest conduction energy bands and the Dirac cones in the surface Brillouin zone disappear. Fig.7(b) and Fig.8(b) show the probability density profiles of the highest valence states with the wave vectors  $(0.6\pi, 0.5\pi)$  and  $(-0.6\pi, 0.5\pi)$ , respectively, from which it is found that the mixing between the surface states on the two opposite boundaries happens due to the existence of the hidden-symmetry-breaking perturbations. Fig.7(c) and Fig.8(c) show the pseudospin textures of the highest valence states, which seem to manifest similar vortex pseudospin textures as the case without hidden-symmetry-breaking perturbations. In fact, for the case with hidden-symmetry-breaking perturbations, the out-of-plane pseudospin component  $\langle s_z \rangle$  appears as shown in Fig.7(d) and Fig.8(d), so the singularity of pseudospin texture disappears and the pseudospin textures are not vortices, which are consistent with the disappearing of the Dirac cones. The above characters confirm that the  $Z_2$  topological insulator and the surface states are protected by the hidden symmetry  $\Upsilon$ .

## VII. EXPERIMENTAL TECHNIQUES FOR REALIZATION AND DETECTION OF THE $Z_2$ TOPOLOGICAL INSULATORS WITH ULTRACOLD ATOMS IN OPTICAL LATTICES

During recent years, ultracold atoms in optical lattices have become a platform to simulate the exotic physics in condensed matters, especially some of which are difficult to realize in real solid materials[26–28]. A lot of experimental techniques have been developed to construct various optical lattices, such as laser-assisting tunneling[29–32], shaking optical lattice[33, 34]. Due to the advantage of ultracold atoms in optical lattices, they have often employed to explore the physics

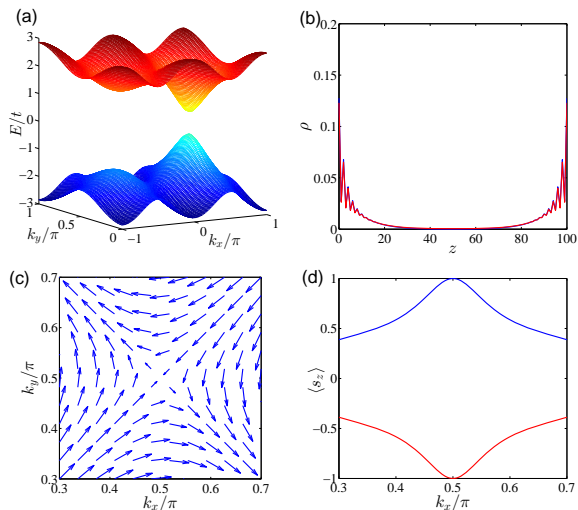


FIG. 7. The properties of the highest valence bands of a slab with the hidden-symmetry-breaking perturbations for the case  $t_1 = 0.3t$ ,  $\lambda = t$ , and  $\mu = 0.8t$ . (a) The dispersion relation; (b) the probability density of the states with the wave vector  $(k_x, k_y) = (0.6\pi, 0.5\pi)$ , where the lines correspond to the two quantum states are entirely overlapped; (c) the pseudospin textures of the average pseudospin components  $(\langle s_x \rangle, \langle s_y \rangle)$  on the  $k_x$ - $k_y$  plane, which are identical and entirely overlapped for two degenerate bands; (d) the profile of the average pseudospin component  $\langle s_z \rangle$  along the  $k_y = 0.5\pi$  line, where the red and blue lines correspond to the two degenerate states, respectively.

of topological phases[35–41]. All of the techniques provide a foundation to design a model to realize a three-dimensional hidden-symmetry-protected  $Z_2$  topological insulator in optical lattices.

In order to realize the model of Eqs.(1), (2), and (3), we select two hyperspin states of cold atoms  ${}^6\text{Li}$  or  ${}^{40}\text{K}$  to be trapped in an cubic optical lattice formed by three pairs of lasers. These two hyperspin states can be regarded as the basis of the color space. The hyperspin-switching hopping can be induced by fine-designed Raman laser fields[29–32]. The accompanying phases of hopping can be realized by tuning the directions and frequencies of assistant lasers[42].

There also many techniques to detect the topological properties in optical lattices. The atomic interferometry is a very useful technique to measure a relative phase. Based on this technique, a direct measurement of the Zak phase in topological Bloch bands was performed[43] and an Aharonov-Bohm interferometer was constructed for determining Bloch band topology[44]. The concrete schemes were designed to measure Chern number[45] and  $Z_2$  topological invariant [46] with atomic interferometry. Very recently, Bloch state tomography was developed to detect Berry curvature and topological invariants, including single- and multiband Chern and  $Z_2$  numbers[47]. Another detecting technique is Bragg spectroscopy[48], which can be employed to probe the dispersion relation of optical lattice. A scheme to detect the edge states based on Bragg scattering was proposed[49]. The edge states can also be detected by direct imaging method[50]. The

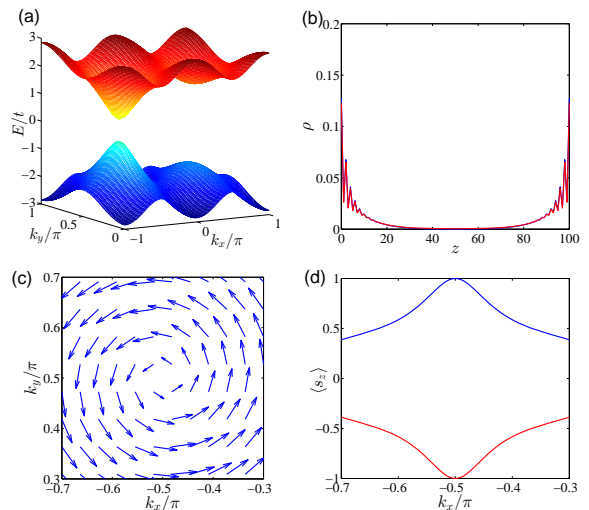


FIG. 8. The properties of the highest valence bands of a slab with the hidden-symmetry-breaking perturbations for the case  $t_1 = 0.3t$ ,  $\lambda = -t$ , and  $\mu = 0.8t$ . (a) The dispersion relation; (b) the probability density of the states with the wave vector  $(k_x, k_y) = (-0.6\pi, 0.5\pi)$ , where the lines correspond to the two quantum states are entirely overlapped; (c) the pseudospin texture of the average pseudospin components  $(\langle s_x \rangle, \langle s_y \rangle)$  on the  $k_x$ - $k_y$  plane, which are identical and entirely overlapped for two degenerate bands; (d) the profile of the average pseudospin component  $\langle s_z \rangle$  along the  $k_y = 0.5\pi$  line, where the red and blue lines correspond to the two degenerate states, respectively.

high-resolution uorescence imaging can probe optical lattices at single-site level[51, 52], so it can be employed to detect edge or surface states by measuring populations of atoms. Based on the above detecting techniques, it is feasible that the  $Z_2$  topological invariant and the surface states in the hidden-symmetry-protected  $Z_2$  topological insulators are measured and detected.

## VIII. CONCLUSION

In summary, we have studied a tight-binding model in a cubic lattice that preserves a hidden symmetry, which has a composite antiunitary operator consisting of fractional translation, complex conjugation, sublattice exchange, and local gauge transformation. Based on the hidden symmetry, we defined a  $Z_2$  topological invariant which classifies the insulator phases of the lattice. In some parameter ranges, the lattice supports a non-trivial topological insulator protected by the hidden symmetry. For the hidden-symmetry-protected topological insulator, the surface states localized on one of open boundaries and have a single Dirac cone band structure on the surface Brillouin zone. We also defined pseudospin operators and find that the surface states have only in-plane components, which form a vortex or antivortex pseudospin texture having a winding number  $\pm 1$ , respectively. When additional hidden-symmetry-breaking perturbations on the open boundaries of a slab geometry are added, an energy gap opens be-

tween the highest valance and lowest conduction bands and the surface states on the two opposite boundaries mix, even turn into bulk states when the perturbations are strong enough. Furthermore, the out-of-plane pseudospin component appears and the singularity of pseudospin texture vanishes. The results of the case with additional hidden-symmetry-breaking perturbations demonstrate that the  $Z_2$  topological insulator and surface states are protected by the hidden symmetry  $\Upsilon$ .

## ACKNOWLEDGMENTS

This work was supported by the National Natural Science Foundation of China under Grants No. 11274061 (J.M.H.) and No. 11504171 (W.C.). W.C. was also supported by the Natural Science Foundation of Jiangsu Province in China under Grant No. BK20150734.

- 
- [1] M. Z. Hasan and C. L. Kane, "Colloquium: Topological insulators," *Rev. Mod. Phys.* **82**, 3045 (2010).
- [2] X.-L. Qi and S.-C. Zhang, "Topological insulators and superconductors," *Rev. Mod. Phys.* **83**, 1057 (2011).
- [3] K. v. Klitzing, G. Dorda, and M. Pepper, "New method for high-accuracy determination of the fine-structure constant based on quantized Hall resistance," *Phys. Rev. Lett.* **45**, 494 (1980).
- [4] D. J. Thouless, M. Kohmoto, M. P. Nightingale, and M. den Nijs, "Quantized Hall conductance in a two-dimensional periodic potential," *Phys. Rev. Lett.* **49**, 405 (1982).
- [5] C. L. Kane and E. J. Mele, "Quantum spin Hall effect in graphene," *Phys. Rev. Lett.* **95**, 226801 (2005).
- [6] C. L. Kane and E. J. Mele, " $Z_2$  topological order and the quantum spin Hall effect," *Phys. Rev. Lett.* **95**, 146802 (2005).
- [7] B. A. Bernevig and S.-C. Zhang, "Quantum spin hall effect," *Phys. Rev. Lett.* **96**, 106802 (2006).
- [8] B. A. Bernevig, T. L. Hughes, and S.-C. Zhang, "Quantum spin hall effect and topological phase transition in hgte quantum wells," *Science* **314**, 1757 (2006).
- [9] M. König, S. Wiedmann, C. Brüne, A. Roth, H. Buhmann, L. W. Molenkamp, X.-L. Qi, and S.-C. Zhang, "Quantum spin hall insulator state in hgte quantum wells," *Science* **318**, 766 (2007).
- [10] L. Fu, C. L. Kane, and E. J. Mele, "Topological insulators in three dimensions," *Phys. Rev. Lett.* **98**, 106803 (2007).
- [11] J. E. Moore and L. Balents, "Topological invariants of time-reversal-invariant band structures," *Phys. Rev. B* **75**, 121306 (2007).
- [12] R. Roy, "Topological phases and the quantum spin Hall effect in three dimensions," *Phys. Rev. B* **79**, 195322 (2009).
- [13] L. Fu and C. L. Kane, "Topological insulators with inversion symmetry," *Phys. Rev. B* **76**, 045302 (2007).
- [14] D. Hsieh, D. Qian, L. Wray, Y. Xia, Y. S. Hor, R. J. Cava, and M. Z. Hasan, "A topological Dirac insulator in a quantum spin Hall phase," *Nature* **452**, 970 (2008).
- [15] Y. Xia, *et al.*, "Observation of a large-gap topological-insulator class with a single Dirac cone on the surface," *Nat. Phys.* **5**, 398 (2009).
- [16] H. Zhang, C.-X. Liu, X.-L. Qi, X. Dai, Z. Fang, and S.-C. Zhang, "Topological insulators in  $\text{Bi}_2\text{Se}_3$ ,  $\text{Bi}_2\text{Te}_3$  and  $\text{Sb}_2\text{Te}_3$  with a single Dirac cone on the surface," *Nat. Phys.* **5**, 438 (2009).
- [17] Y. L. Chen, *et al.*, "Experimental realization of a three-dimensional topological insulator,  $\text{Bi}_2\text{Te}_3$ ," *Science* **325**, 178 (2009).
- [18] D. Hsieh, *et al.*, "A tunable topological insulator in the spin helical Dirac transport regime," *Nature* **460**, 1101 (2009).
- [19] D. Hsieh, *et al.*, "Observation of time-reversal-protected single-Dirac-cone topological-insulator states in  $\text{Bi}_2\text{Te}_3$  and  $\text{Sb}_2\text{Te}_3$ ," *Phys. Rev. Lett.* **103**, 146401 (2009).
- [20] L. Fu, "Topological crystalline insulators," *Phys. Rev. Lett.* **106**, 106802 (2011).
- [21] T. H. Hsieh, H. Lin, J. Liu, W. Duan, A. Bansil, and L. Fu, "Topological crystalline insulators in the SnTe material class," *Nat. Commun.* **3**, 982 (2012).
- [22] C.-X. Liu, R.-X. Zhang, and B. K. VanLeeuwen, "Topological nonsymmorphic crystalline insulators," *Phys. Rev. B* **90**, 085304 (2014).
- [23] J.-M. Hou, "Hidden-symmetry-protected topological semimetals on a square lattice," *Phys. Rev. Lett.* **111**, 130403 (2013).
- [24] J.-M. Hou, "Moving and merging of Dirac points on a square lattice and hidden symmetry protection," *Phys. Rev. B* **89**, 235405 (2014).
- [25] J.-M. Hou and W. Chen, "Hidden-symmetry-protected quantum pseudo-spin Hall effect in optical lattices," *Phys. Rev. A* **93**, 063626 (2016).
- [26] D. Jaksch and P. Zoller, "The cold atom Hubbard toolbox," *Ann. Phys.* **315**, 52 (2005).
- [27] I. Bloch, J. Dalibard, and W. Zwerger, "Many-body physics with ultracold gases," *Rev. Mod. Phys.* **80**, 885 (2008).
- [28] M. Lewenstein, A. Sanpera, V. Ahufinger, B. Damski, A. Sen, and U. Sen, "Ultracold atomic gases in optical lattices: mimicking condensed matter physics and beyond," *Adv. Phys.* **56**, 243 (2007).
- [29] M. Aidelsburger, M. Atala, S. Nascimbène, S. Trotzky, Y.-A. Chen, and I. Bloch, "Experimental realization of strong effective magnetic fields in an optical lattice," *Phys. Rev. Lett.* **107**, 255301 (2011).
- [30] M. Aidelsburger, M. Atala, M. Lohse, J. T. Barreiro, B. Paredes, and I. Bloch, "Realization of the Hofstadter hamiltonian with ultracold atoms in optical lattices," *Phys. Rev. Lett.* **111**, 185301 (2013).
- [31] H. Miyake, G. A. Siviloglou, C. J. Kennedy, W. C. Burton, and W. Ketterle, "Realizing the Harper hamiltonian with laser-assisted tunneling in optical lattices," *Phys. Rev. Lett.* **111**, 185302 (2013).
- [32] Z. Wu, L. Zhang, W. Sun, X.-T. Xu, B.-Z. Wang, S.-C. Ji, Y. Deng, S. Chen, X.-J. Liu, and J.-W. Pan, "Realization of two-dimensional spin-orbit coupling for Bose-Einstein condensates," *Science* **354**, 83 (2016).
- [33] J. Struck, C. Ölschläger, M. Weinberg, P. Hauke, J. Simonet, A. Eckardt, M. Lewenstein, K. Sengstock, and P. Windpassinger, "Tunable gauge potential for neutral and spinless particles in driven optical lattices," *Phys. Rev. Lett.* **108**, 225304 (2012).
- [34] J. Struck, *et al.*, "Engineering ising-XY spin-models in a triangular lattice using tunable artificial gauge fields," *Nat. Phys.* **9**, 738 (2013).
- [35] N. Goldman, J. C. Budich, and P. Zoller, "Topological quantum matter with ultracold gases in optical lattices," *Nat. Phys.* **12**, 639 (2016).

- [36] N. Goldman, A. Kubasiak, A. Bermudez, P. Gaspard, M. Lewenstein, and M. A. Martin-Delgado, “Non-abelian optical lattices: Anomalous quantum Hall effect and Dirac fermions,” *Phys. Rev. Lett.* **103**, 035301 (2009).
- [37] N. Goldman, I. Satija, P. Nikolic, A. Bermudez, M. A. Martin-Delgado, M. Lewenstein, and I. B. Spielman, “Realistic time-reversal invariant topological insulators with neutral atoms,” *Phys. Rev. Lett.* **105**, 255302 (2010).
- [38] G. Liu, S.-L. Zhu, S. Jiang, F. Sun, and W. M. Liu, “Simulating and detecting the quantum spin Hall effect in the kagome optical lattice,” *Phys. Rev. A* **82**, 053605 (2010).
- [39] C. J. Kennedy, G. A. Siviloglou, H. Miyake, W. C. Burton, and W. Ketterle, “Spin-orbit coupling and quantum spin Hall effect for neutral atoms without spin flips,” *Phys. Rev. Lett.* **111**, 225301 (2013).
- [40] A. Bermudez, L. Mazza, M. Rizzi, N. Goldman, M. Lewenstein, and M. A. Martin-Delgado, “Wilson fermions and axion electrodynamics in optical lattices,” *Phys. Rev. Lett.* **105**, 190404 (2010).
- [41] B. Béri and N. R. Cooper, “ $Z_2$  topological insulators in ultracold atomic gases,” *Phys. Rev. Lett.* **107**, 145301 (2011).
- [42] W. Chen, H.-Z. Lu, and J.-M. Hou, “Topological semimetals with a double-helix nodal link,” *Phys. Rev. B* **96**, 041102 (2017).
- [43] M. Atala, M. Aidelsburger, J. T. Barreiro, D. Abanin, T. Kitagawa, E. Demler, and I. Bloch, “Direct measurement of the Zak phase in topological Bloch bands,” *Nat. Phys.* **9**, 795 (2013).
- [44] L. Duca, T. Li, M. Reitter, I. Bloch, M. Schleier-Smith, and U. Schneider, “An Aharonov-Bohm interferometer for determining Bloch band topology,” *Science* **347**, 288 (2015).
- [45] D. A. Abanin, T. Kitagawa, I. Bloch, and E. Demler, “Interferometric approach to measuring band topology in 2D optical lattices,” *Phys. Rev. Lett.* **110**, 165304 (2013).
- [46] F. Grusdt, D. Abanin, and E. Demler, “Measuring  $Z_2$  topological invariants in optical lattices using interferometry,” *Phys. Rev. A* **89**, 043621 (2014).
- [47] T. Li, L. Duca, M. Reitter, F. Grusdt, E. Demler, M. Endres, M. Schleier-Smith, I. Bloch, and U. Schneider, “Bloch state tomography using Wilson lines,” *Science* **352**, 1094 (2016).
- [48] D. M. Stamper-Kurn, A. P. Chikkatur, A. Görlitz, S. Inouye, S. Gupta, D. E. Pritchard, and W. Ketterle, “Excitation of phonons in a Bose-Einstein condensate by light scattering,” *Phys. Rev. Lett.* **83**, 2876 (1999).
- [49] N. Goldman, J. Beugnon, and F. Gerbier, “Detecting chiral edge states in the Hofstadter optical lattice,” *Phys. Rev. Lett.* **108**, 255303 (2012).
- [50] N. Goldman, J. Dalibard, A. Dauphin, F. Gerbier, M. Lewenstein, P. Zoller, and I. B. Spielman, “Direct imaging of topological edge states in cold-atom systems,” *Proc. Natl. Acad. Sci. U.S.A.* **110**, 6736 (2013).
- [51] W. S. Bakr, A. Peng, M. E. Tai, R. Ma, J. Simon, J. I. Gillen, S. Fölling, L. Pollet, and M. Greiner, “Probing the superfluid-to-Mott insulator transition at the single-atom level,” *Science* **329**, 547 (2010).
- [52] J. F. Sherson, C. Weitenberg, M. Endres, M. Cheneau, I. Bloch, and S. Kuhr, “Single-atom-resolved fluorescence imaging of an atomic Mott insulator,” *Nature* **467**, 68 (2010).